Li *et al.*
Chinese Journal of Mechanical Engineering (2023) 36:73
https://doi.org/10.1186/s10033-023-00906-5

Chinese Journal of Mechanical Engineering

ORIGINAL ARTICLE

Open Access

Smooth Trajectory Planning for a Cable Driven Parallel Waist Rehabilitation Robot Based on Rehabilitation Evaluation Factors

Yuan Li[1], Bin Zi[1*], Zhi Sun[1] and Ping Zhao[1]

Abstract

Rehabilitation robots can help physiatrists to assist patients in improving their movement ability. Due to the interaction between rehabilitation robots and patients, the robots need to complete rehabilitation training on a safe basis. This paper presents an approach for smooth trajectory planning for a cable-driven parallel waist rehabilitation robot (CDPWRR) based on the rehabilitation evaluation factors. First, motion capture technology is used to collect the motion data of several volunteers in waist twisting. Considering the impact of motion variability, the feature points at the center of the human pelvis are obtained after eliminating unreasonable data through rationality judgments. Then, point-to-point waist training trajectory planning based on quintic polynomial and cycloid functions, and multipoint waist training trajectory planning based on quintic B-spline functions are carried out. The corresponding planned curves and kinematics characteristics using three methods are compared and analyzed. Subsequently, the rehabilitation evaluation factors are introduced to conduct smooth trajectory planning for waist training, and the waist trajectory with better compliance is obtained based on the safety and feasibility of waist motion. Finally, the physical prototype of the CDPWRR is built, and the feasibility and effectiveness of the proposed smooth trajectory planning method are proved by numerical analysis and experiments.

Keywords Waist rehabilitation robot, Trajectory planning, B-spline, Rehabilitation evaluation factor

1 Introduction

In recent years, with the increasing trend of social aging, the number of stroke patients has increased accordingly [1]. The symptoms of waist impairments commonly occur in stroke patients. Research on modern rehabilitation medicine and neuroscience show that task-oriented repetitive movements can improve muscle strength and coordination in patients with motor dysfunction [2]. With the help of rehabilitation robots, patients can regain the ability of waist movement through repeated gait, sit-up or waist-twisting training [3, 4]. Due to the interaction between rehabilitation robots and patients, the robots need to complete rehabilitation training on a safe basis [5, 6]. The effect of waist rehabilitation is related to some factors, such as the intensity of rehabilitation training and the flexibility of rehabilitation movement. Therefore, the rehabilitation trajectory should be designed based on the motion of human waist.

To develop rehabilitation robots and training trajectories more suitable for patients, research on human motion models has been carried out [7]. It is found that the complexity of human motion cannot be simply defined as a combination of several degrees of freedom, which deviates from the real needs of rehabilitation patients [8–10]. Varela et al. [11] proposed a cable-based parallel manipulator system CaTraSys to measure the kinematic characteristics of human walking. Hu et al. [12] considered the rotation of human waist and

*Correspondence:
Bin Zi
zibinhfut@163.com
[1] School of Mechanical Engineering, Hefei University of Technology, Hefei 230009, China

estimated the human walking speed using a wearable accelerometer. Martín et al. [13] detected and identified six postural transitions using an inertial sensor located at the human waist. The cross-section average method is widely used in the time alignment processing for data series to reduce the impact of movement variability in the human body, which eliminates the inherent change characteristics of the data and ignores the drift of the center point to a certain extent [14].

The collected information on human motion is essentially a series of discrete position points, which needs further trajectory planning. The trajectory planning problem in 3-D space contains point-to-point trajectory planning with determined initial and end points, and multi-point trajectory planning by interpolating or approximating a set of via-points [15–18]. In point-to-point trajectory planning, polynomial, cycloid, and trigonometric function curves are commonly used to define trajectories [19]. Each segment can be optimized separately to obtain specific kinematic characteristics. Multi-point trajectory planning is a global optimization problem [20–23]. The approaches mainly include polynomial functions of proper degree and B-spline functions. Gosselin [24] presented an approach for dynamic trajectory planning of 3-DOF spatial cable-suspended parallel robots using periodic functions, which can guarantee that cable tensions remain positive throughout the trajectory. Jiang et al. [25] conducted point-to-point dynamic trajectory planning for a 6-DOF cable-suspended parallel robot, which can generate the trajectory beyond the static workspace of the robot. Li et al. [26] presented an approach for smooth trajectory planning of a 4-DOF SCARA using quintic B-splines to achieve C4-continuity. Abbasnejad et al. [27] designed a 4-4 planar cable-driven parallel robot for gait rehabilitation and optimized the gait trajectory with the particle swarm algorithm.

In summary, the current research on human motion models is mostly related to the gait characteristics in normal walking, running or abnormal walking, and the research on motion characteristics in waist twisting is relatively limited. In addition, due to the interaction between rehabilitation robots and the human body, the motion trajectory needs to ensure compliance based on the safety and comfort of patients. Therefore, the mentioned trajectory planning method needs further study.

In this paper, an approach for smooth trajectory planning for a cable-driven parallel waist rehabilitation robot (CDPWRR) based on the rehabilitation evaluation factors is proposed. Considering the impact of movement variability, the feature points at the center of the human pelvis are obtained after collecting and processing waist motion data. The prototype of the CDPWRR is built, and the feasibility of the proposed method is verified by numerical analysis and experiments. This paper is arranged as follows. In Section 2, the waist motion data of several male adults in waist twisting are collected, and the waist feature points are obtained. In Section 3, the waist training trajectories are generated by the quintic polynomial, cycloid and quintic B-spline functions, respectively. In Section 4, the rehabilitation evaluation factors are introduced, and the smooth trajectory planning for waist training on the CDPWRR is conducted. Subsequently, the feasibility and effectiveness of the proposed method are verified on the physical prototype. Conclusions are drawn in Section 5.

2 Acquisition of Waist Motion Feature Points

20 male adults are chosen as the volunteers, and the Nokov optical motion capture system mainly composed of 8 infrared cameras is used to capture the motion data of the human waist [28]. 4 markers are evenly placed at the waist of volunteers, which are located at the front, back, left and right directions, respectively. The joints of upper and lower limbs are used as auxiliary points. Before the experiment, volunteers need to perform the slow counterclockwise rotation movement of the waist with the maximum range. The principle of waist motion measurement is shown in Figure 1.

After the post-processing in Cortex, the data of waist twisting have variability, which is similar to the data of human gait. After segmenting the original data and fitting them with Fourier functions, the rationality of the characteristic parameters such as the number of collected points, the fitting residuals and the deviations of key fitting parameters are judged. The unreasonable data are eliminated through various rationality judgments, and the key parameters are averaged to obtain the final fitting results. The fitting functions in X and Y directions can be expressed as:

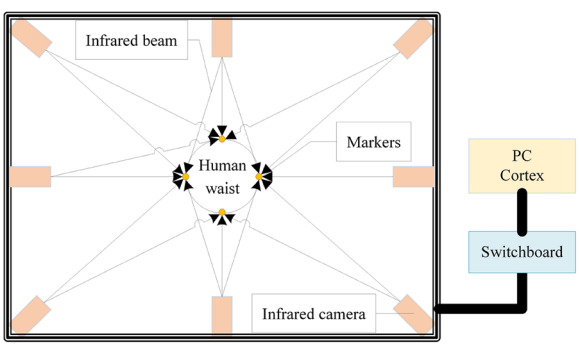

Figure 1 Principle of waist motion measurement

$$f_x = a_x + a'_x \sin(\omega i), \tag{1}$$

$$f_y = a_y + a'_y \sin\left(\omega i + \pi/2\right), \tag{2}$$

where a_x and a_y are the coordinates of the center point of the fitting trajectory, respectively. a'_x and a'_y are the amplitudes in X and Y directions, respectively. ω is the fitting frequency.

Take the data collected from Volunteer 1 as an example. Due to the different number of points collected in each waist twisting cycle, the key fitting parameters are obtained by fitting the data segment of each waist twisting cycle separately. After distinguishing the number of data points of each data segment, the fitting results of key parameters in X and Y directions are shown in Tables 1 and 2, respectively. According to normal distribution guidelines, the 3σ values of key parameters are obtained after removing the maximum and minimum values. In Table 1, the data in the 10th segment is judged as an abnormal segment, and the fitting data are averaged

Table 1 Key fitting parameters of each waist twisting cycle in *X* direction

Waist twisting cycles	Key fitting parameters					R-squares	Removal conditions
	a_0	a_1	b_1	ω	a'_x		
1st	7.6832	38.4680	− 4.8989	0.0536	38.7787	0.9806	Excessive fitting residual
2nd	8.2234	44.8662	0.5078	0.0446	44.8691	0.9935	
3rd	9.3725	38.0859	− 6.5433	0.0501	38.6439	0.9963	
4th	6.2964	35.6410	− 2.1783	0.0477	35.7075	0.9821	Excessive fitting residual
5th	9.3321	30.8377	− 2.6001	0.0553	30.9472	0.9967	
6th	8.9843	30.2105	1.8983	0.0510	30.2701	0.9950	
7th	6.6655	33.2023	− 2.3185	0.0453	33.2832	0.9992	
8th (min)	4.6415	31.8730	− 10.8424	0.0476	33.6667	0.9888	Excessive fitting residual
9th	6.5133	30.2323	− 0.9434	0.0568	30.2470	0.9962	
10th (max)	13.9039	29.7146	− 10.1172	0.0473	31.3897	0.9932	$>3\sigma$
11th	8.3610	36.1557	3.4668	0.0484	36.3216	0.9943	
12th	9.7264	28.8197	5.8161	0.0542	29.4007	0.9885	Excessive fitting residual
13th	11.2816	34.8355	− 6.7973	0.0487	35.4925	0.9969	
14th	8.2762	39.7236	− 4.3227	0.0486	39.9581	0.9939	
15th	9.8185	33.7732	− 3.2430	0.0556	33.9285	0.9996	

Table 2 Key fitting parameters of each waist twisting cycle in *Y* direction

Waist twisting cycles	Key fitting parameters					R-squares
	a_0	a_1	b_1	ω	a'_x	
1st	10.0903	40.5181	− 45.6060	0.0502	61.0051	0.9967
2nd	9.7610	45.2876	1.4728	0.0531	45.3116	0.9977
3rd	1.6601	56.3211	7.5311	0.0497	56.8224	0.9992
4th	3.5996	58.8380	7.3858	0.0507	59.2998	0.9976
5th	10.7859	57.8365	1.6622	0.0487	57.8603	0.9978
6th	9.6217	54.5511	0.4017	0.0501	54.5526	0.9997
7th	13.1768	56.8928	− 7.5860	0.0485	57.3963	0.9987
8th (min)	11.6342	57.4316	13.8960	0.0506	59.0888	0.9986
9th	14.2717	57.2698	− 2.0050	0.0527	57.3049	0.9926
10th (max)	16.0207	61.1319	− 2.9088	0.0484	61.2011	0.9986
11th	14.2903	54.8039	− 18.0752	0.0474	57.7077	0.9901
12th	16.1964	55.7053	3.0875	0.0503	55.7908	0.9959
13th	13.1907	46.6916	6.4250	0.0564	47.1316	0.9990

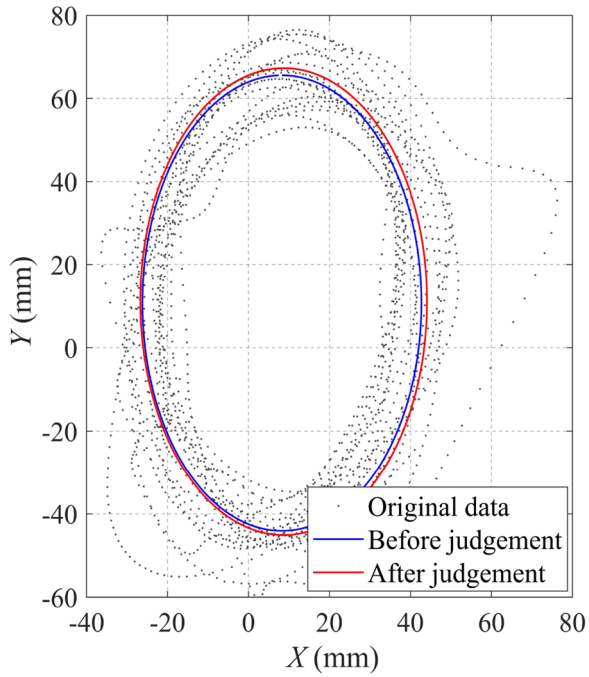

Figure 2 Comparison of fitting results in the horizontal plane

after removing it. Finally, the accurate fitting result of the waist trajectory is obtained.

Figure 2 shows the comparison of the fitting results of the waist motion in the horizontal plane before and after the rationality judgement. It can be seen from Figure 2 that the results obtained after removing the abnormal data are closer to the real situation. By judging the rationality of the data, the problems of different amounts of data points and fitting frequency in each cycle are solved, and the drift of the center point is fully considered to a certain extent.

Based on this, the fitting results of the waist motion trajectory in the horizontal plane are obtained. The center point of the human waist in a standing state, and the center point of the human waist at the front, back, left and right endpoints in the waist twisting are selected as feature points, which are noted as $A_1(0,0,0)$, $A_2(a_x^{'},0,h_1)$, $A_3(0,a_y^{'},h_2)$, $A_4(-a_x^{'},0,h_1)$ and $A_5(0,-a_y^{'},h_2)$, respectively.

3 Generation of Waist Training Trajectory

The feature points obtained in Section 2 are represented in Figure 3. The projection of the waist motion path of seven feature points with determined coordinates in the horizontal plane is composed of two line segments and an ellipse. Points A_1 and A_7 are the start and end points of the trajectory, respectively. Points A_1 and A_7, A_2 and A_6 are coincident, respectively. Points $A_{2(6)}$, A_3, A_4 and A_5 are the endpoints of the ellipse. The set of all passing points is symmetric about A_1A_2, and the sequence of each point is $A_1(0,0,0)$, $A_2(a_x^{'},0,h_1)$, $A_3(0,a_y^{'},h_2)$, $A_4(-a_x^{'},0,h_1)$, $A_5(0,-a_y^{'},h_2)$, $A_6(a_x^{'},0,h_1)$, $A_7(0,0,0)$. $a_x^{'}$ and $a_y^{'}$ denote the endpoint values on the short axis and long axis of the ellipse, respectively. h_1 and h_2 denote the Z-axis coordinates at the corresponding endpoints, respectively. The fitting data of Volunteer 2 with acceptable dispersion and relatively large amplitude of waist twisting are selected as the feature points in trajectory planning. At this time, the values of $a_x^{'}$ and $a_y^{'}$ are 78 mm and 102.5 mm, respectively. And the length H of human lower limbs is 1100 mm. According to the selected feature points, the motion path of the center of the human waist is shown in Figure 3.

The trajectory of the center of human waist can be expressed as:

$$X=\begin{cases}\frac{a_x^{'}}{t_1}t, 0\le t\le t_1,\\ a_x^{'}\cdot\sin\left[\omega(t-t_1)+\pi/2\right], t_1<t\le t_2,\\ a_x^{'}-\frac{a_x^{'}}{t_1}(t-t_2), t_2<t\le t_1+t_2,\end{cases}\quad(3)$$

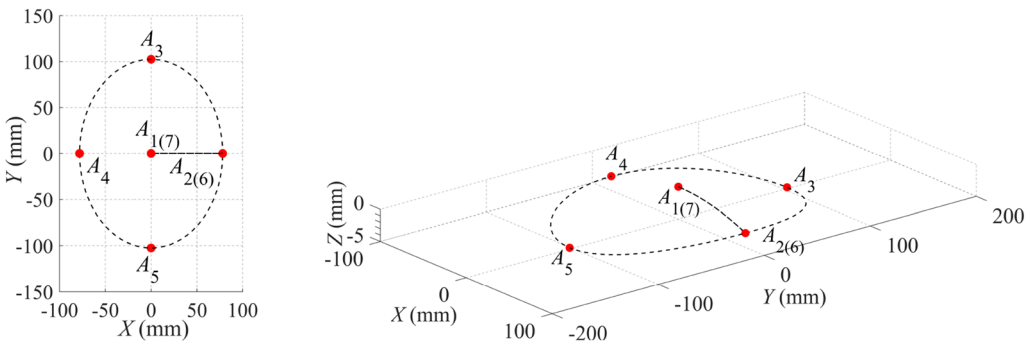

(a) Path in the horizontal plane (b) Path in 3D space

Figure 3 A given waist path defined in Cartesian space

$$Y = \begin{cases} 0, 0 \le t \le t_1, \\ a_y' \cdot \sin\left[\omega(t - t_1)\right], t_1 < t \le t_2, \\ 0, t_2 < t \le t_1 + t_2, \end{cases} \tag{4}$$

$$Z = \sqrt{H^2 - X^2 - Y^2} - H, 0 < t \le t_1 + t_2, \tag{5}$$

where a_x' and a_y' are the endpoint values on the short axis and long axis of the ellipse, respectively. ω denotes the frequency. t_1 denotes the time from A_1 to A_2. The time scale factor is defined as $k_t = 4t_1/t_2$.

3.1 Point-to-Point Waist Training Trajectory Planning

Point-to-point waist training trajectory planning based on quintic polynomial functions can ensure continuous acceleration, and the displacement can be expressed as:

$$\begin{aligned} f(t) = {} & f_0 + k_1(t - t_0) + k_2(t - t_0)^2 \\ & + k_3(t - t_0)^3 + k_4(t - t_0)^4 + k_5(t - t_0)^5, \end{aligned} \tag{6}$$

where t_0, f_0, v_0 and a_0 denote the initial time, displacement, velocity and acceleration of each trajectory segment, respectively. t_f, f_f, v_f and a_f denote the final time, displacement, velocity and acceleration of each trajectory segment, respectively.

The formulas of velocity, acceleration and jerk can be expressed as:

$$\begin{aligned} \dot{f}(t) = {} & k_1 + 2k_2(t - t_0) + 3k_3(t - t_0)^2 \\ & + 4k_4(t - t_0)^3 + 5k_5(t - t_0)^4, \end{aligned} \tag{7}$$

$$\ddot{f}(t) = 2k_2 + 6k_3(t - t_0) + 12k_4(t - t_0)^2 + 20k_5(t - t_0)^3, \tag{8}$$

$$\dddot{f}(t) = 6k_3 + 24k_4(t - t_0) + 60k_5(t - t_0)^2. \tag{9}$$

The time and displacement of each trajectory segment are defined as $\Delta T = t_f - t_0$ and $\Delta f = f_f - f_0$, respectively. The coefficients in Eqs. (6)–(9) can be expressed as:

$$\begin{cases} k_1 = v_0, \\ k_2 = \dfrac{a_0}{2}, \\ k_3 = \dfrac{20\Delta f - (12v_0 + 8v_f)\Delta T - (3a_0 - a_f)\Delta T^2}{2\Delta T^3}, \\ k_4 = \dfrac{-30\Delta f + (16v_0 + 14v_f)\Delta T + (3a_0 - 2a_f)\Delta T^2}{2\Delta T^4}, \\ k_5 = \dfrac{12\Delta f - 6(v_0 + v_f)\Delta T - (a_0 - a_f)\Delta T^2}{2\Delta T^5}. \end{cases} \tag{10}$$

When using quintic polynomial functions to plan the waist training trajectory in three axes, setting the speeds and accelerations in Z-axis at points A_2 and A_6 as 0 for subsection planning is not consistent with the real situations. Therefore, the trajectory segment from A_1 to A_3, the segment from A_3 to A_4, the segment from A_4 to A_5 and the segment from A_5 to A_7 are planned, respectively. At this time, the planned waist training trajectory does not pass through points $A_{2(6)}$. By setting the constraint conditions at points $A_{2(6)}$, the training trajectory can pass through points $A_{2(6)}$. The displacements, velocities, accelerations and jerks of the training trajectory planned by quintic polynomial functions in X, Y and Z directions can be optimized by choosing the total time T and time scale factor k_t.

Point-to-point waist training trajectory planning based on cycloid functions can ensure continuous acceleration, and its displacement can be expressed as:

$$p(t) = (p_f - p_0)\left(\frac{t - t_0}{t_f - t_0} - \frac{1}{2\pi}\sin\frac{2\pi(t - t_0)}{t_f - t_0}\right) + p_0, \tag{11}$$

where t_0 and p_0 denote the initial time and displacement of each trajectory segment, respectively. t_f and f_f denote the final time and displacement of each trajectory segment, respectively.

The time and displacement of each trajectory segment are defined as $\Delta T = t_f - t_0$ and $\Delta p = p_f - p_0$, respectively. Thus Eq. (11) can be rewritten as:

$$p(t) = \Delta p\left(\frac{t - t_0}{\Delta T} - \frac{1}{2\pi}\sin\frac{2\pi(t - t_0)}{\Delta T}\right) + p_0. \tag{12}$$

The formulas of velocity, acceleration and jerk can be expressed as:

$$\dot{p}(t) = \frac{\Delta p}{\Delta T}\left(1 - \cos\frac{2\pi(t - t_0)}{\Delta T}\right), \tag{13}$$

$$\ddot{p}(t) = \frac{2\pi\Delta p}{\Delta T^2}\sin\frac{2\pi(t - t_0)}{\Delta T}, \tag{14}$$

$$\dddot{p}(t) = \frac{4\pi^2\Delta p}{\Delta T^3}\cos\frac{2\pi(t - t_0)}{\Delta T}. \tag{15}$$

The waist training trajectory does not pass through points $A_{2(6)}$ when using cycloid functions to plan the waist training trajectory in three axes, which is similar to the result using quintic polynomial functions. Similarly, by setting the constraint conditions at points $A_{2(6)}$, the training trajectory can pass through points $A_{2(6)}$. The displacements, velocities, accelerations and jerks of the training trajectory planned by cycloid functions in X, Y and Z directions can be optimized by choosing the total time T and time scale factor k_t.

3.2 Multipoint Waist Training Trajectory Planning

Multipoint waist training trajectory planning based on quintic B-spline functions can ensure continuous change rate of acceleration [29], and the general form of B-spline functions can be expressed as:

$$\boldsymbol{S}(u) = \sum_{i=0}^{m} \boldsymbol{P}_i B_i^k(u), \tag{16}$$

where $\boldsymbol{P}_i$ denotes the set of control points of B-spline functions, and the number of control points is $m+1$. $B_i^k(u)$ denotes the basis function of degree k defined for the knot vector $\boldsymbol{U} = \{u_0, \cdots, u_{n_{knot}}\}$. The knot vector $\boldsymbol{U}$ is a monotone non-decreasing sequence of real numbers, and the number of knots is $n_{knot}+1$. $n_{knot} = m+k+1$.

The i-th B-spline basis function of degree k can be expressed as:

$$B_i^0(u) = \begin{cases} 1, \text{ if } u_i \le u \le u_{i+1}, \\ 0, \text{ otherwise}, \end{cases}$$

$$B_i^k(u) = \frac{u-u_i}{u_{i+k}-u_i} B_i^{k-1}(u) + \frac{u_{i+k+1}-u}{u_{i+k+1}-u_{i+1}} B_{i+1}^{k-1}(u), \tag{17}$$

where define $0/0 = 0$.

According to the properties of B-spline functions, the r-order derivative can be expressed as:

$$S^{(r)}(u) = \sum_{i=0}^{m} P_i B_i^{k(r)}(u), \tag{18}$$

where

$$\begin{cases} B_i^{k(r)}(u) = \dfrac{k!}{(k-r)!} \displaystyle\sum_{j=0}^{r} a_{r,j} B_{i+j}^{k-r}, \\ a_{0,0} = 1, \\ a_{r,0} = \dfrac{a_{r-1,0}}{u_{i+k-r+1}-u_i}, \\ a_{r,j} = \dfrac{a_{r-1,j}-a_{r-1,j-1}}{u_{i+k+j-r+1}-u_{i+j}}, j = 1, \ldots, r-1, \\ a_{r,r} = \dfrac{-a_{r-1,r-1}}{u_{i+k+1}-u_{i+r}}. \end{cases} \tag{19}$$

$P_i (i = 0, \cdots, m)$ and $B_i^k(u)$ need to be determined first when using quintic B-spline functions to plan the waist training trajectory. $Q_s (s = 0, \cdots, n)$ and T are set as the via-points and the total time, respectively. $\tau_s (s = 0, \cdots, n)$ represents the time nodes of the via-points after normalizing. Generally, for B-spline functions with k order (k is odd), the knot vector $\boldsymbol{U} = \{u_0, \cdots, u_{n_{knot}}\}$ can be written as:

$$\boldsymbol{U} = \left\{ \underbrace{\tau_0, ..., \tau_0}_{k+1}, \tau_1, \ldots, \tau_{n-1}, \underbrace{\tau_n, \ldots, \tau_n}_{k+1} \right\}, \tag{20}$$

where $n_{knot}+1 = n+1+2k$, and the number of vis-points is $n+1$. $\tau_0 = 0, \tau_n = 1$.

Thus the equation of the via-points of the waist training trajectory can be expressed as:

$$S(\tau_s) = Q_s. \tag{21}$$

The position equations of the via-points can be expressed as:

$$\begin{cases} Q_s = \left[B_0^k(\tau_s), B_1^k(\tau_s), \ldots, B_{m-1}^k(\tau_s), B_m^k(\tau_s) \right] \begin{bmatrix} P_0 \\ P_1 \\ \vdots \\ P_{m-1} \\ P_m \end{bmatrix}, \\ s = 0, \ldots, n. \end{cases} \tag{22}$$

To obtain the constraints about velocity and acceleration, Eq. (18) can be rewritten as:

$$S^{(r)}(\tau_s) = \sum_{i=0}^{m} P_i B_i^{k(r)}(\tau_s). \tag{23}$$

Eq. (23) can be expanded as:

$$S^{(r)}(\tau_s) = \left[B_0^{k(r)}(\tau_s), B_1^{k(r)}(\tau_s), \ldots, B_{m-1}^{k(r)}(\tau_s), B_m^{k(r)}(\tau_s) \right] \begin{bmatrix} P_0 \\ P_1 \\ \vdots \\ P_{m-1} \\ P_m \end{bmatrix}. \tag{24}$$

Therefore, the constraints about velocity and acceleration can be expressed as:

$$v_s = \left[B_0^{k(1)}(\tau_s), B_1^{k(1)}(\tau_s), \ldots, B_{m-1}^{k(1)}(\tau_s), B_m^{k(1)}(\tau_s) \right] \begin{bmatrix} P_0 \\ P_1 \\ \vdots \\ P_{m-1} \\ P_m \end{bmatrix}, \tag{25}$$

$$a_s = \left[B_0^{k(2)}(\tau_s), B_1^{k(2)}(\tau_s), \ldots, B_{m-1}^{k(2)}(\tau_s), B_m^{k(2)}(\tau_s) \right] \begin{bmatrix} P_0 \\ P_1 \\ \vdots \\ P_{m-1} \\ P_m \end{bmatrix}. \tag{26}$$

According to Eqs. (21)–(26), the constraints of via-points can be rewritten as:

$$\boldsymbol{AP} = \boldsymbol{c}, \tag{27}$$

where

$$\boldsymbol{A} = \begin{bmatrix} B_0^k(\tau_0) & B_1^k(\tau_0) & \cdots & B_m^k(\tau_0) \\ B_0^{k(1)}(\tau_0) & B_1^{k(1)}(\tau_0) & \cdots & B_m^{k(1)}(\tau_0) \\ B_0^{k(2)}(\tau_0) & B_1^{k(2)}(\tau_0) & \cdots & B_m^{k(2)}(\tau_0) \\ B_0^k(\tau_1) & B_1^k(\tau_1) & \cdots & B_m^k(\tau_1) \\ \vdots & \vdots & \ddots & \vdots \\ B_0^k(\tau_{n-1}) & B_1^k(\tau_{n-1}) & \cdots & B_m^k(\tau_{n-1}) \\ B_0^{k(2)}(\tau_n) & B_1^{k(2)}(\tau_n) & \cdots & B_m^{k(2)}(\tau_n) \\ B_0^{k(1)}(\tau_n) & B_1^{k(1)}(\tau_n) & \cdots & B_m^{k(1)}(\tau_n) \\ B_0^k(\tau_n) & B_1^k(\tau_n) & \cdots & B_m^k(\tau_n) \end{bmatrix}_{(n+5)\times(m+1)}, \tag{28}$$

$$\boldsymbol{P} = [P_0, P_1, \ldots, P_{m-1}, P_m]^{\mathrm{T}}, \tag{29}$$

$$\boldsymbol{c} = [Q_0, v_0, a_0, Q_1, \ldots, Q_{n-1}, a_n, v_n, Q_n]^{\mathrm{T}}. \tag{30}$$

The characteristics of the planned waist training trajectory can be optimized by adjusting the distribution of τ_s in Eq. (20). Points A_1–A_7 are set as via-points in multipoint waist training trajectory planning based on quintic B-spline functions. Virtual via-points are set near the initial and end points, respectively. The knot vector of the quintic B-spline functions in Eq. (20) can be rewritten as:

$$\boldsymbol{U} = \{0, 0, 0, 0, 0, 0, \tau_1, \ldots, \tau_7, 1, 1, 1, 1, 1, 1\}, \tag{31}$$

where $\tau_1 = 0.125k_a$, $\tau_2 = 0.25k_b$, $\tau_3 = 0.375$, $\tau_4 = 0.5$, $\tau_5 = 0.625$, $\tau_6 = 1 - 0.25k_b$, $\tau_7 = 1 - 0.125k_a$. k_a and k_b are two node parameters of the quintic B-spline functions. $0 < k_a \leq 1, 0.5 \leq k_b \leq 1.5$.

3.3 Numerical Analysis

In this section, numerical analysis is performed to demonstrate the effectiveness of the proposed trajectory planning methods. The total time T and the time scale factor k_t are set to 40 s and 1, respectively. The displacements, velocities, accelerations and jerks of the waist training trajectory in X direction planned by quintic polynomial functions are shown in Figure 4. The displacements, velocities, accelerations and jerks of the waist training trajectory in Y direction planned by cycloid functions are shown in Figure 5. When $k_a = k_b = 1$, the nodes in the knot vector is uniformly distributed. The displacements, velocities, accelerations and jerks of the waist training trajectory in Z direction planned by quintic B-spline functions are shown in Figure 6.

Actually, in X, Y and Z directions, the displacement and velocity curves of the waist training trajectories at points $A_{2(6)}$ after point-to-point waist training trajectory planning based on quintic polynomial and cycloid functions realize the smooth transition. The accelerations and jerks at the turning points are significantly reduced, avoiding the vibration and impact problems caused by the sudden change to a certain extent, and preventing secondary injury in rehabilitation training. Point-to-point waist training trajectory planning based on quintic polynomial and cycloid functions ensures that the velocities and accelerations at both ends of the waist training trajectories start from zero. The compliances of velocities are guaranteed, and the accelerations and jerks are greatly reduced. However, the jerks at both ends of the waist training trajectories cannot be guaranteed to start from zero. The waist training trajectories do not pass through points $A_{2(6)}$ using point-to-point waist training trajectory planning based on quintic polynomial and cycloid functions.

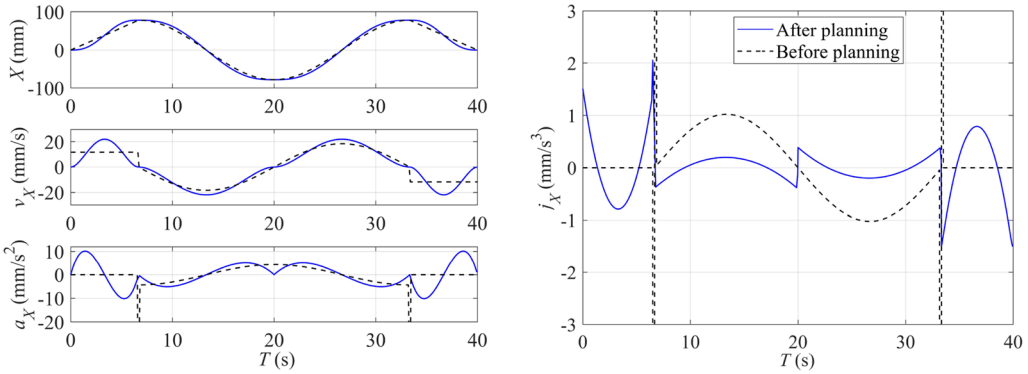

(a) Displacement, velocity, acceleration curves (b) Jerk curves

Figure 4 Displacements, velocities, accelerations and jerks of the waist training trajectory in X direction after quintic polynomial planning

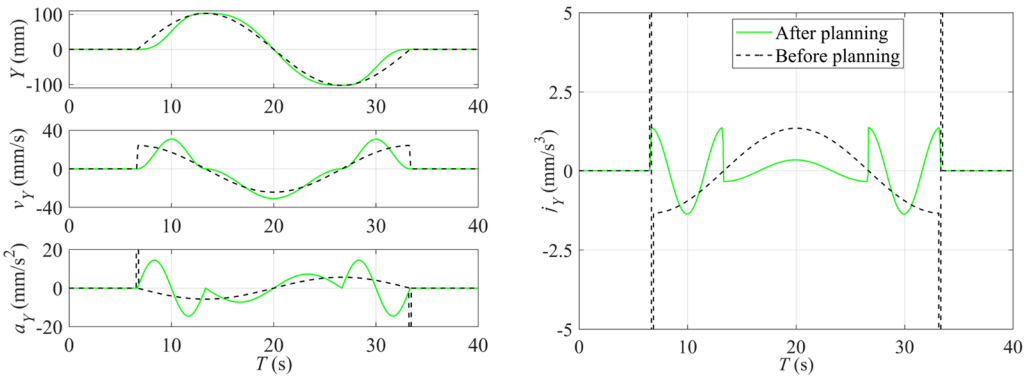

(a) Displacement, velocity, acceleration curves (b) Jerk curves

Figure 5 Displacements, velocities, accelerations and jerks of the waist training trajectory in *Y* direction after cycloid planning

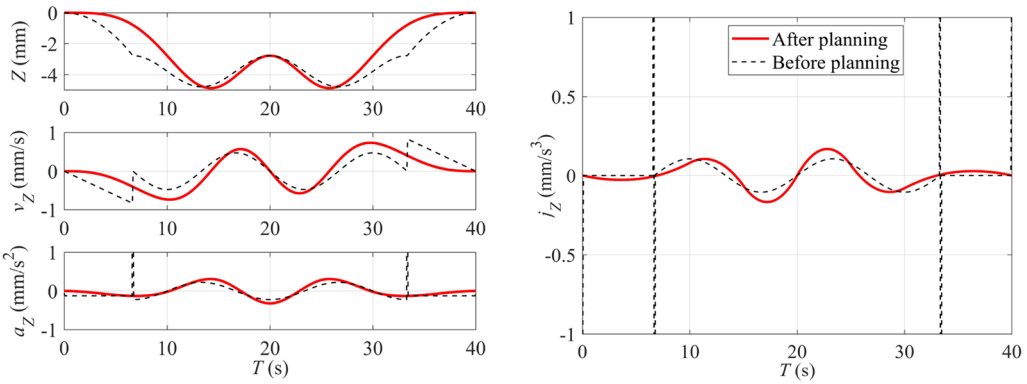

(a) Displacement, velocity, acceleration curves (b) Jerk curves

Figure 6 Displacements, velocities, accelerations and jerks of the waist training trajectory in *Z* direction after quintic B-spline planning

In *X*, *Y* and *Z* directions, the displacement, velocity, acceleration and jerk curves of the waist training trajectory at points $A_{2(6)}$ after multipoint waist training trajectory planning based on quintic B-spline functions realize the smooth transition. Compared with the results of point-to-point waist training trajectory planning, multipoint waist training trajectory planning based on quintic B-spline functions ensures that the accelerations and jerks at both ends of the waist training trajectories start from zero. The compliances of accelerations and jerks are guaranteed, greatly reducing the vibration and impact problems caused by the sudden change at the turning point, and avoiding the secondary injury in rehabilitation training. The waist training trajectory passes through points $A_{2(6)}$ using multipoint waist training trajectory planning based on quintic B-spline functions. The waist training trajectories generated by quintic polynomial, cycloid and quintic B-spline functions are shown in Figure 7.

4 Smooth Trajectory Planning Considering Rehabilitation Evaluation Factors

4.1 Smooth Trajectory Planning for the CDPWRR

As mentioned above, the acceleration and jerk curves of the waist training trajectory planned by quintic B-spline functions are smooth without mutation compared with the results of point-to-point waist training trajectory planning. Based on this, the smooth trajectory planning for waist training considering the influence of human lower limbs is conducted. According to Eq. (31), the planned waist training trajectory can be determined by the two node parameters k_a and k_b of the quintic B-spline functions, and the total time *T*.

To realize the equivalent waist movement, a CDPWRR is built to complete the rehabilitation training. The rehabilitation robot needs to complete the training trajectory based on ensuring safety. When planning the waist training trajectory, the constraints of human lower limbs on the CDPWRR cannot be ignored. In Section 3, the length *H* of human lower limbs is set as 1100 mm.

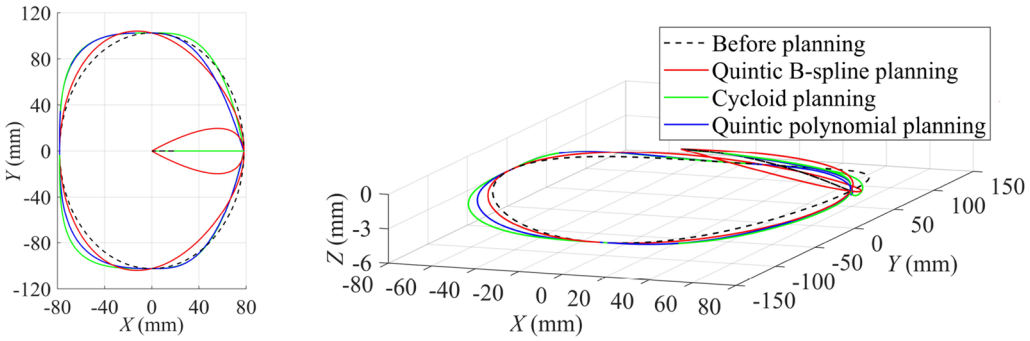

(a) Trajectory in the horizontal plane (b) Trajectory in 3D space

Figure 7 Waist trajectory before and after planning

However, in the actual process of waist twisting, there exists bending in human lower limbs. The actual length H_0 of the human lower limbs is defined as:

$$H_0 = H_1 + H_2, \tag{32}$$

$$\cos\delta = \frac{H_1^2 + H_2^2 - H^2}{2H_1H_2}, \tag{33}$$

where H_1 and H_2 are the lengths of the upper and lower parts of human lower limbs, respectively. δ is the joint angle of human lower limbs.

Based on the above analysis, the actual length H_0 of human lower limbs should be kept in a certain range to make the joint angle of human lower limbs in a reasonable range, ensuring the safety of humans in the process of rehabilitation training. Therefore, the evaluation factor of joint comfort is introduced as one of the rehabilitation evaluation factors, as shown in Eq. (34):

$$h_{\max}(k_a, k_b) = \max_{0\le\tau\le1} |\boldsymbol{h}(\tau)|. \tag{34}$$

Similarly, the actual rotation angle α of human waist should be kept in a reasonable range. The evaluation factor of waist comfort is introduced as one of the rehabilitation evaluation factors, as shown in Eq. (35):

$$\alpha_{\max}(k_a, k_b) = \max_{0\le\tau\le1} |\boldsymbol{\alpha}(\tau)|. \tag{35}$$

In addition, smooth jerk curves without mutation can reduce the impact on human body and ensure the safety in rehabilitation training. The maximum value of jerks in rehabilitation training is set as the evaluation factor of compliance. Then the evaluation factor of compliance is introduced as one of the rehabilitation evaluation factors, as shown in Eq. (36):

$$j_{\max}(k_a, k_b) = \max_{0\le\tau\le1} \left|\boldsymbol{j}(\tau)\right|. \tag{36}$$

From Eqs. (34)–(36), the variations of the rehabilitation evaluation factors $h_{\max}$, $\alpha_{\max}$ and $j_{\max}$ with two node parameters k_a and k_b can be obtained, as shown in Figure 8.

The rehabilitation evaluation factors $h_{\max}$ and $\alpha_{\max}$ are taken as constraints, and $j_{\max}$ is taken as the optimization objective in order to ensure safety and feasibility in rehabilitation training. The optimal smooth trajectory planning for waist training considering rehabilitation evaluation factors is obtained by the following optimization function:

$$\begin{aligned} &\min j_{\max}(k_a, k_b) = \max_{0\le\tau\le1} \left|\boldsymbol{j}(\tau)\right|, \\ &\text{s.t. } 0 < k_a \le 1, \\ &0.5 \le k_b \le 1.5, \\ &850 \le h_{\max}(k_a, k_b) \le 1250, \\ &\alpha_{\max}(k_a, k_b) \le \pi/8. \end{aligned} \tag{37}$$

When k_a equals to 0.32 and k_b is taken as 0.8, the optimal solution of smooth trajectory planning for waist training considering rehabilitation evaluation factors is obtained, which is 3.1929 mm/s^3. The waist training trajectories and jerks before and after optimization in X, Y and Z directions are shown in Figure 9.

It is clear from Figure 9 that the peak jerks of the optimized waist training trajectory the X, Y and Z directions decrease to a certain extent. The standard deviations of the jerks before and after optimization are

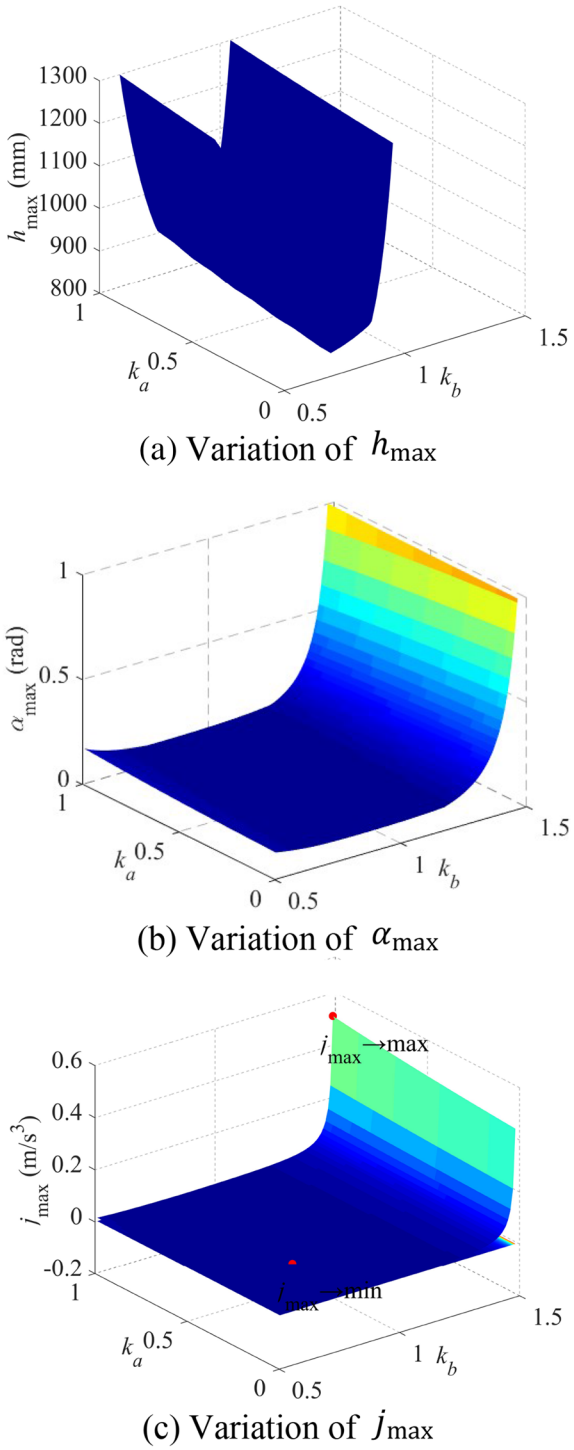

Figure 8 Variations of h_{max}, α_{max} and j_{max} with k_a and k_b

1.402 and 0.644, respectively. The result after optimization is less than that before optimization. The rehabilitation evaluation factors $h_{max}(k_a, k_b)$ and $\alpha_{max}(k_a, k_b)$ before and after optimization are 1455 mm, 879 mm, 0.096 rad and 0.094 rad, respectively. According to Eq. (37), the rehabilitation evaluation factors of the optimized waist training trajectory are within the reasonable ranges, ensuring the safety and feasibility of waist training.

4.2 Verification on the CDPWRR

Both numerical analysis and experiments are carried out on the CDPWRR to verify the effectiveness and feasibility of the proposed approach. The 3D model and physical prototype of the CDPWRR are shown in Figure 10. The standing platform is driven by four cables to promote the lower limbs, achieving the equivalent movement of the human waist [30].

To ensure safety and reveal a more obvious effect, the values of a_x' and a_y' are set as 93 mm combined with the actual dimensions and performance of the physical prototype. The total time T is set to 56 s. The initial length H_0 of human lower limbs is set to 360 mm. In this example, the range of rehabilitation evaluation factor h_{max} is set from 300 to 450. We set k_a equal to 0.33, and k_b is taken as 0.86, the optimal solution of smooth trajectory planning for waist training considering rehabilitation evaluation factors is obtained. The optimized waist training trajectory for the CDPWRR is shown in Figure 11. The theoretical and experimental lengths, and the length errors of four cables are shown in Figure 12.

Compared with the theoretical values, the maximum length errors of four cables in the experiments are 5.94 mm, 3.10 mm, 6.18 mm and 5.50 mm, respectively. The jerks before and after optimization are 1.8395 mm/s^3 and 1.2315 mm/s^3, respectively. The rehabilitation evaluation factors $h_{max}(k_a, k_b)$ and $\alpha_{max}(k_a, k_b)$ of the optimized waist training trajectory are 339.7 mm and 0.2802 rad, respectively. The values of rehabilitation evaluation factors are within the reasonable ranges, which proves the feasibility and effectiveness of the proposed trajectory planning method.

5 Conclusions

(1) The waist motion data are collected using motion capture technology. Aimed at the impact of motion variability, the unreasonable data are eliminated through rationality judgments, and the key parameters are processed to obtain the feature points at the center of human pelvis.

(2) The quintic polynomial, cycloid, and quintic B-spline functions are used for waist trajectory planning, respectively. The results of trajectory planning using three methods are compared and analyzed. Compared with the results of point-

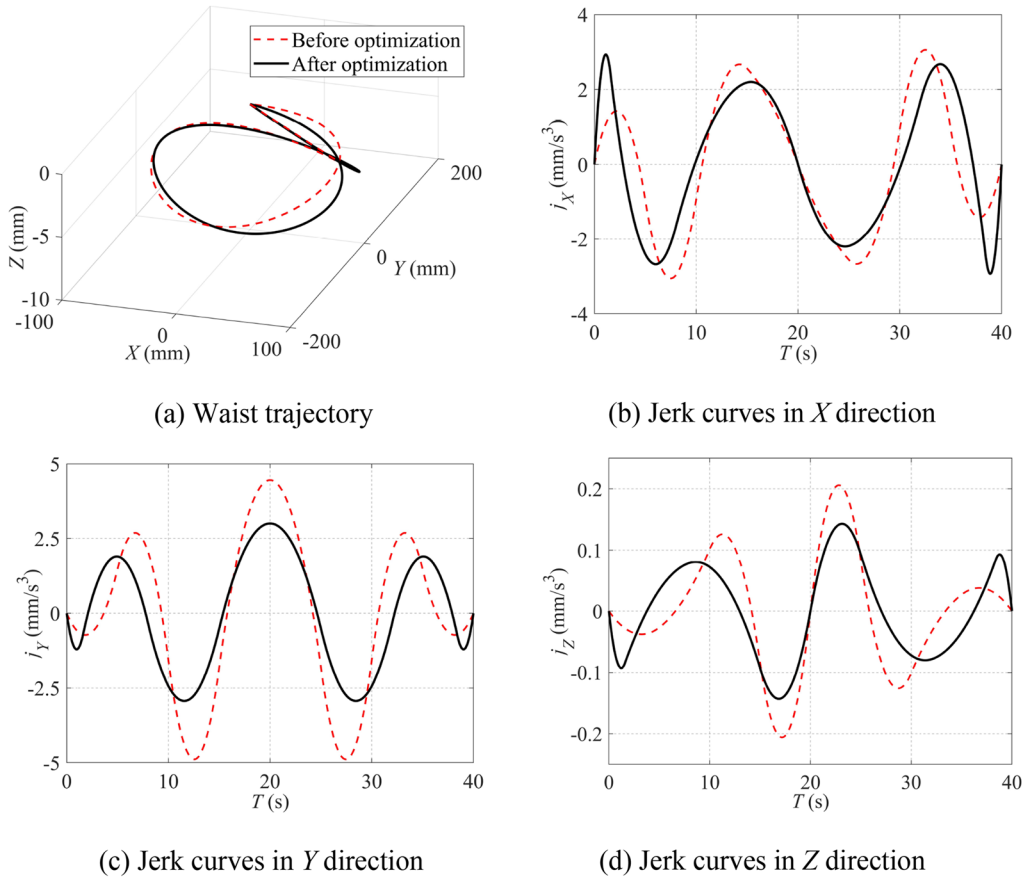

(a) Waist trajectory

(b) Jerk curves in X direction

(c) Jerk curves in Y direction

(d) Jerk curves in Z direction

Figure 9 Waist trajectory and jerk curves before and after optimization

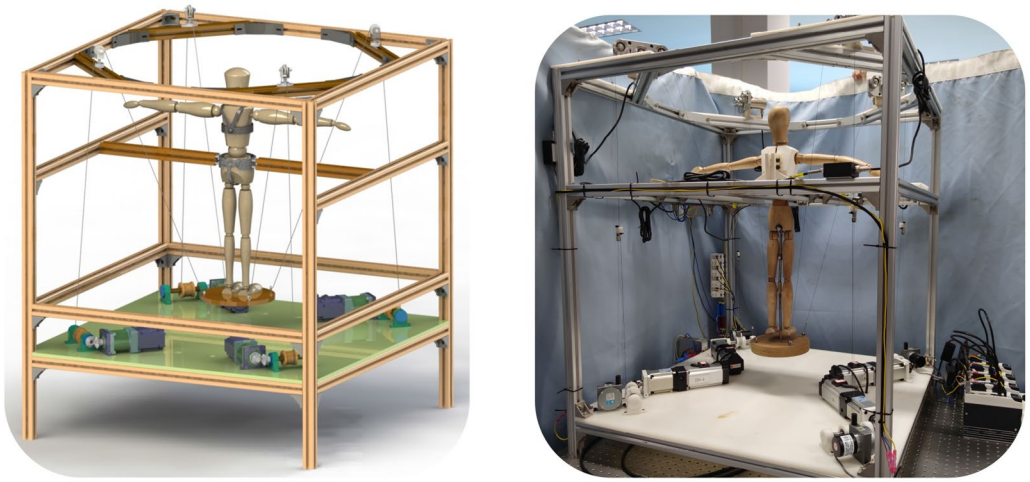

(a) 3D model

(b) Physical prototype

Figure 10 3D model and physical prototype of the CDPWRR

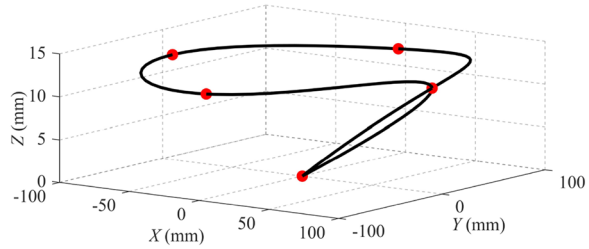

Figure 11 The optimized waist training trajectory for the CDPWRR

to-point waist training trajectory planning, the acceleration and jerk curves of the waist training trajectory planned by quintic B-spline functions are smooth without mutation.

(3) In order to complete the waist training trajectory on the basis of ensuring safety, three rehabilitation evaluation factors are introduced to conduct smooth trajectory planning. The waist trajectory with better compliance is obtained based on the safety of waist motion.

(4) A CDPWRR is built to implement the equivalent waist rehabilitation training. The results of numerical analysis and experiments verify the feasibility and effectiveness of the proposed smooth trajectory planning method for waist training.

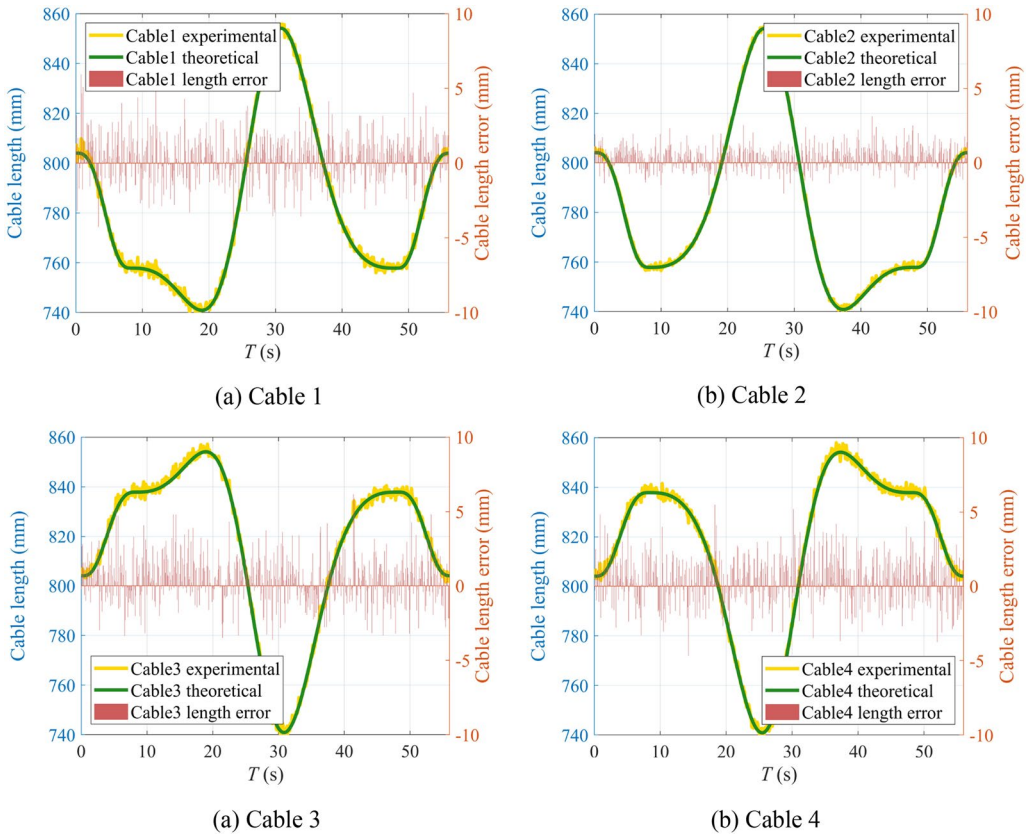

Figure 12 The lengths and length errors of four cables

Acknowledgements
Not applicable.

Author Contributions
BZ was in charge of the whole trial; YL designed the experiments and wrote the manuscript; ZS assisted with experimental setup; PZ assisted with structure and language of the manuscript. All authors read and approved the final manuscript.

Authors' Information
Yuan Li, is currently a lecturer at *School of Mechanical Engineering, Hefei University of Technology, China*. She received the PhD degree from *Hefei University of Technology, China*, in 2021. Her research interests include robotics and automation, and rehabilitation robots.
Bin Zi, is currently a professor, the Dean of *School of Mechanical Engineering*, and the Director of *Robotics Institute, Hefei University of Technology, China*. He received the PhD degree from *Xidian University, China*, in 2007. His research interests include robotics and automation, mechatronics, and multi-robot systems.
Zhi Sun, is currently a PhD candidate at *School of Mechanical Engineering, Hefei University of Technology, China*. His research interests include mechanism design and control technology of robots.
Ping Zhao, is currently a professor at *School of Mechanical Engineering, Hefei University of Technology, China*. She received the PhD degree from *Stony Brook University, USA*, in 2013. Her research interests include mechanism and robotics, and rehabilitation robots.

Funding
Supported by National Natural Science Foundation of China (Grant Nos. 52205014, 51925502), and the Fundamental Research Funds for the Central Universities (Grant Nos. JZ2022HGTA0325, JZ2022HGQA0147).

Declarations

Competing interests
The authors declare no competing financial interests.

Received: 23 July 2022 Revised: 9 June 2023 Accepted: 12 June 2023
Published online: 21 June 2023

References

[1] M S Ekker, J I Verhoeven, I Vaartjes, et al. Stroke incidence in young adults according to age, subtype, sex, and time trends. *Neurology*, 2019, 92(21): e2444-e2454.
[2] J Dąbrowski, A Czajka, J Zielińska-Turek, et al. Brain functional reserve in the context of neuroplasticity after stroke. *Neural Plasticity*, 2019: 9708905.
[3] B Zi, Y Li. Conclusions in theory and practice for advancing the applications of cable-driven mechanisms. *Chinese Journal of Mechanical Engineering*, 2017, 30(4): 763-765.
[4] Q Chen, B Zi, Z Sun, et al. Design and development of a new cable-driven parallel robot for waist rehabilitation. *IEEE/ASME Transactions on Mechatronics*, 2019, 24(4): 1497-1507.
[5] C Nicholson-Smith, V Mehrabi, S F Atashzar, et al. A multi-functional lower-and upper-limb stroke rehabilitation robot. *IEEE Transactions on Medical Robotics and Bionics*, 2020, 2(4): 549-552.
[6] F Lanotte, Z McKinney, L Grazi, et al. Adaptive control method for dynamic synchronization of wearable robotic assistance to discrete movements: Validation for use case of lifting tasks. *IEEE Transactions on Robotics*, 2021, 37(6): 2193-2209.
[7] D Shi, W Zhang, W Zhang, et al. A review on lower limb rehabilitation exoskeleton robots. *Chinese Journal of Mechanical Engineering*, 2019, 32(1): 1-11.
[8] Y Pei, R H Ewoldt, C M Zallek, et al. Design framework and clinical evaluation of a passive hydraulic patient simulator for biceps spasticity assessment training. *Journal of Mechanisms and Robotics*, 2021, 13(4): 041006.
[9] B Kim, U Jeong, B B Kang, et al. Slider-tendon linear actuator with under-actuation and fast-connection for soft wearable robots. *IEEE/ASME Transactions on Mechatronics*, 2021, 26(6): 2932-2943.
[10] Y L Wang, K Y Wang, W Y Zhao, et al. Effects of single crouch walking gaits on fatigue damages of lower extremity main muscles. *Journal of Mechanics in Medicine and Biology*, 2019, 19(07): 1940046.
[11] M J Varela, M Ceccarelli, P Flores. A kinematic characterization of human walking by using CaTraSys. *Mechanism and Machine Theory*, 2015, 86: 125-139.
[12] J S Hu, K C Sun, C Y Cheng. A kinematic human-walking model for the normal-gait-speed estimation using tri-axial acceleration signals at waist location. *IEEE Transactions on Biomedical Engineering*, 2013, 60(8): 2271-2279.
[13] D R Martín, A Samá, C P López, et al. Identification of postural transitions using a waist-located inertial sensor. *International Work-Conference on Artificial Neural Networks*, Puerto de la Cruz, Spain, June 12–14, 2013: 142–149.
[14] K Davids, S Bennett, K M Newell. *Movement system variability*. Champaign: Human Kinetics, 2006.
[15] H Wang, H Wang, J Huang, et al. Smooth point-to-point trajectory planning for industrial robots with kinematical constraints based on high-order polynomial curve. *Mechanism and Machine Theory*, 2019, 139: 284-293.
[16] S Xiang, H Gao, Z Liu, et al. Dynamic transition trajectory planning of three-DOF cable-suspended parallel robots via linear time-varying MPC. *Mechanism and Machine Theory*, 2020, 146: 103715.
[17] S Baressi Šegota, N Anđelić, I Lorencin, et al. Path planning optimization of six-degree-of-freedom robotic manipulators using evolutionary algorithms. *International Journal of Advanced Robotic Systems*, 2020, 17(2): 1729881420908076.
[18] T Chettibi. Smooth point-to-point trajectory planning for robot manipulators by using radial basis functions. *Robotica*, 2019, 37(3): 539-559.
[19] E Idà, T Bruckmann, M Carricato. Rest-to-rest trajectory planning for underactuated cable-driven parallel robots. *IEEE Transactions on Robotics*, 2019, 35(6): 1338-1351.
[20] E Barnett, C Gosselin. A bisection algorithm for time-optimal trajectory planning along fully specified paths. *IEEE Transactions on Robotics*, 2020, 37(1): 131-145.
[21] F Yuan, D Chen, C Pan, et al. Application of optimal-jerk trajectory planning in gait-balance training robot. *Chinese Journal of Mechanical Engineering*, 2022, 35(1): 1-12.
[22] S Qian, K Bao, B Zi, et al. Dynamic trajectory planning for a three degrees-of-freedom cable-driven parallel robot using quintic B-splines. *Journal of Mechanical Design*, 2020, 142(7): 073301.
[23] Y Fang, J Hu, W Liu, et al. Smooth and time-optimal S-curve trajectory planning for automated robots and machines. *Mechanism and Machine Theory*, 2019, 137: 127-153.
[24] C Gosselin. Global planning of dynamically feasible trajectories for three-DOF spatial cable-suspended parallel robots. *Cable-Driven Parallel Robots*. Heidelberg: Springer, 2013: 3–22.
[25] X Jiang, E Barnett, C Gosselin. Dynamic point-to-point trajectory planning beyond the static workspace for six-dof cable-suspended parallel robots. *IEEE Transactions on Robotics*, 2018, 34(3): 781-793.
[26] Y Li, T Huang, D G Chetwynd. An approach for smooth trajectory planning of high-speed pick-and-place parallel robots using quintic B-splines. *Mechanism and Machine Theory*, 2018, 126: 479-490.
[27] G Abbasnejad, J Yoon, H Lee. Optimum kinematic design of a planar cable-driven parallel robot with wrench-closure gait trajectory. *Mechanism and Machine Theory*, 2016, 99: 1-18.
[28] Y Li, Z Yang, M Jiang, et al. Path planning for a cable-driven parallel waist rehabilitation robot based on discriminant analysis model. *2021 IEEE International Conference on Electrical Engineering and Mechatronics Technology (ICEEMT)*, Qingdao, China, July 2–4, 2021: 439–444.
[29] L Biagiotti, C Melchiorri. *Trajectory planning for automatic machines and robots*. Heidelberg: Springer Science & Business Media, 2008.
[30] Y Li, B Zi, B Zhou, et al. Cable angle and minimum resultant force response analysis of lower limb traction device for rehabilitation robot with interval parameters. *Journal of Computing and Information Science in Engineering*, 2021, 21(2): 021002.